

NuSTAR discovery of a cyclotron line in GRO J1750-27

Ashwin Devaraj^{1,2}[★] and Biswajit Paul¹[†]

¹Raman Research Institute, Sadashivnagar, Bangalore-560080, India

²Joint Astronomy Programme, Indian Institute of Science, Bangalore-560012, India

Accepted XXX. Received YYY; in original form ZZZ

ABSTRACT

GRO J1750-27, discovered during an outburst in 1995 with CGRO-BATSE, is one of the farthest known Be-X-ray binary systems. This relatively poorly studied system recently went into an outburst. From the measurements of the spin-up rate of this pulsar, the X-ray fluxes during the two previous outbursts in 2008 and 2014-2015, and using the standard theory of accretion torque on magnetized neutron stars, the magnetic field strength was estimated to be 2×10^{12} G and $3.5 - 4.5 \times 10^{12}$ G respectively. The uncertainty in the distance causes large uncertainty in the estimated magnetic field. The source was observed during the latest outburst using the *NuSTAR* telescope during the rising phase of the outburst. We estimate the spin period of the source to be 4.45s using which we produced energy resolved pulse profiles between 3 and 79 keV. We find that the profiles appear to be double peaked at low energies (<20 keV) while evolving into a single peak at higher energies (>20 keV). The broadband spectrum of this source was described by a power-law modified by an exponential cut off and we report the discovery of a cyclotron resonant scattering feature (CRSF) in this hard X-ray spectrum of this source at 43 keV indicating a magnetic field strength of 3.7×10^{12} G. Our estimate of the magnetic field strength using the cyclotron line is consistent with the estimate made using the accretion torque model.

Key words: keyword1 – keyword2 – keyword3

1 INTRODUCTION

Be/X-ray binaries (BeXRB) are a sub-class of High Mass X-ray Binaries (HMXB) are systems that host a Neutron Star (NS) and a fast rotating B-type main sequence companion that also exhibit emission lines from the circumstellar disc around the companion (Reig 2011). GRO J1750-27 (also known as AX J1749.1-2639) is one such transient system discovered by the *CGRO/BATSE* during an outburst that lasted about two months in 1995 (Koh et al. 1995; Scott et al. 1997). Coherent pulsations of 4.45s interpreted as the spin period and a 29.8 day orbital period was reported by Scott et al. (1997) using the same data. Though no optical counterpart was detected, based on the position of this source on the Corbet diagram, Scott et al. (1997) concluded that the system must be a BeXRB.

The source once again underwent an outburst around Jan. 2008, which lasted for ~ 150 days, during which it was observed with *INTEGRAL* and *Swift XRT* (Shaw et al. 2009). Along with providing an updated orbital ephemeris, Shaw et al. (2009) also modelled the broadband spectrum of GRO J1750-27 with a cutoff power-law, estimating a flux of 6.5×10^{-9} erg cm⁻² s⁻¹ in the 0.1 - 100 keV range. Using the spin-up rate and pulsed flux determined from the *Swift/BAT* data and applying the Ghosh & Lamb model (Ghosh & Lamb 1978), they estimated a surface magnetic field of $B \sim 2 \times 10^{12}$ G and a distance range of 12 - 22 kpc.

This source's third Type II outburst began in Dec. 2014 and lasted

up to May 2015 (Finger & Wilson-Hodge 2014; Lutovinov et al. 2019). During this period it was also observed with *Chandra*, *Swift* and *Fermi* using which Lutovinov et al. (2019) accurately measured the coordinates of the source to be R.A. = 17^h49^m12.99^s, Dec. = -26°38'38.5" (in the J2000 system) and identified an IR counterpart at a distance of >12 kpc. Analysing the spin evolution of GRO J1750-27, they also provide an independent distance estimate to be between 14 and 22 kpc with the expected magnetic field strength to be in the range $(3.5 - 4.5) \times 10^{12}$ G. They also conclude that the companion must be an early B-type star using data from the VVV/ESO and UKIDSS/GPS surveys. Rouco Escorial et al. (2019) studied the object during quiescence after the 2015 outburst, using *Swift/XRT* and *Chandra* data to investigate the cooling of the heated NS crust post the outburst and conclude that the X-ray emission is likely due to low-level accretion rather than being due to the cooling.

Once again, on 18 September 2021, GRO J1750-27 began to exhibit another major outburst and coherent pulsations of 4.45s were detected by *Fermi/GBM* (Malacaria et al. 2021). In this work, we discuss this source's spectral and timing analysis using a *NuSTAR* observation that was made during this outburst and report the discovery of a cyclotron line at ~ 43 keV.

2 OBSERVATIONS AND DATA REDUCTION

The most recent outburst of this source began on 18 September 2021, and was still ongoing at the time of the preparation of this manuscript. 15 - 50 keV *Swift/BAT* light curves of the source's outburst are

[★] ashwin@rri.res.in

[†] bpaul@rri.res.in

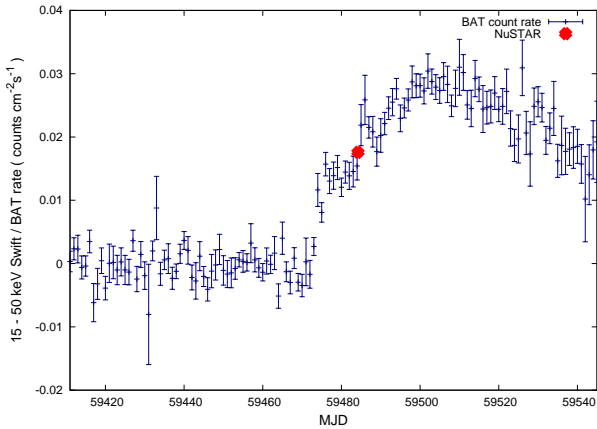


Figure 1. *Swift*/BAT light curve of the 2021 outburst in the 15 - 50 keV range. Blue points indicate the *Swift*/BAT count rate while the red diamond indicates the *NuSTAR* observation. The data were obtained from <https://swift.gsfc.nasa.gov/results/transients/weak/AXJ1749.1-2639>

available, and a 30 ks *NuSTAR* observation was made on the 27th September 2021 (OBSID:90701331002), during the rising phase of the outburst (see Fig. 1). The source continued to brighten till it reached a maximum flux of almost twice the flux measured during the time of this *NuSTAR* observation.

The *Nuclear Spectroscopic Telescope Array* (*NuSTAR*) is a hard X-ray telescope with two identical focal plane modules (FPMA and FPMB), each containing four solid-state CdZnTe detectors, sensitive in the 3 - 79 keV range (Harrison et al. 2013). Its spectral resolution is ~ 0.4 keV at 10 keV and around 0.9 keV at 60 keV. It has a Wolter-I geometry in which the X-rays are focused on the detector by being reflected at grazing angles on an arrangement of paraboloid and hyperboloid mirrors. There are cases where the X-rays from off-axis sources get reflected off only one of the mirrors before reaching the detectors, and these give rise to Ghost rays in the image (Madsen et al. 2017). This *NuSTAR* observation of GRO J1750-27 suffers from this effect, as can be seen in Fig. 2.

The *NuSTAR* data was reduced in the standard way using HEASOFT v6.29c, NUSTARDAS v2.1.1 (CALDB version:20211020). The *nupipeline* script was used to produce the filtered event files. The source region was selected with a radius of 100 arcsec as shown in Fig. 2. Due to the source region being contaminated by the photons from the Ghost Rays (GRs), the choice of background needed to be made more carefully, and it is clear that the GRs are identically present in both FPMA and FPMB as can be seen in Fig. 2. Mainly, Streak II and a portion of Streak I contaminate the source region that we have chosen. In order to identify an appropriate background region that would have approximately the same number of GR photons, we selected consecutive circular regions of 28 arcsec radius along each streak and estimated the flux. We found that the flux drops identically along each streak as a function of the distance from the edge of the detector. Based on this we identified the position (BKG_B) on Streak IV where the intensity of the streak should be approximately equal to the intensity of Streak II when it reaches the Source region. Two more regions adjacent to BKG_B, i.e., BKG_A and BKG_C, were selected along the Streak IV to understand how significantly the choice of background would affect the spectral analysis. The spectra of the source and three background regions were extracted using the *nuproducts* script and can be seen in Fig. 3. It is clear from the figure that the black and blue curves that represent the spectra from regions BKG_A and BKG_B are very similar while

the magenta curves representing the spectra from region BKG_C is slightly higher than the other two up to ~ 20 keV. Above 20 keV, all the backgrounds are quite similar. Above 65 keV, the source and background count rates all become comparable, thus limiting our spectral analysis to the 3 - 65 keV range.

For the timing analysis, the *nuproducts* script was used on the barycenter corrected, filtered event files to produce the light curves with a time resolution of 0.01s for both FPMA and FPMB. Using the *1cmath* script we produced background-subtracted light curves with the choice of the background being BKG_B. For the spectral analysis, the spectra were optimally binned based on the scheme given by Kaastra & Bleeker (2016) and fit simultaneously with the relative normalisation between the two modules being allowed to freely vary (fixing the FPMA's normalisation constant to unity). This cross normalisation was found to be $C_B \sim 1.01$. The spectral analysis was carried out using *XSPEC* version 12.12.0.

3 ANALYSIS AND RESULTS

3.1 Timing Analysis

We found the spin period of the source, $P_{\text{spin}} = 4.451271 \pm 2 \times 10^{-6}$ s using the epoch folding χ^2 maximization technique using the *ef-search* tool which is a part of the FTOOLS package. The quoted (1σ) uncertainty was determined by identifying the difference of trial periods one would have to move for the maximum χ^2 value to reduce by one standard deviation of a wide range of chi-square values for trial periods far from the peak.

3.1.1 Energy-resolved Pulse Profiles

The energy-resolved pulse profiles were generated for the 3 - 9 keV, 9 - 18 keV, 18 - 28 keV, 28 - 38 keV, 38 - 48 keV, 48 - 65 keV energy ranges by folding the light curves of each of these ranges at the determined P_{spin} value. The light curves from both FPMA and FPMB were added using the *1cmath* routine prior to the folding. The pulse profiles have a complex evolution with the increase in energy (see Fig. 4). As also noted by (Shaw et al. 2009), the pulse profiles have a multi-peaked structure in the lower energy ranges (< 20 keV) while it evolves into a single-peaked structure above 20 keV. In particular, the 9 - 18 keV pulse profile seems to have a more complex shape than the 3 - 9 keV one in that the minima of the former seems to appear earlier than the latter. There is also another small maxima at around the phase of 0.6 apart from the biggest peak at phase ~ 0.7 as can be seen in panel (2) of Fig. 4. The pulse profiles in the ranges above 18 keV have a single-peaked structure. It is interesting to note that the minima in of the 18 - 28 keV profiles appear at a phase of ~ 1.2 (see panel (3)), unlike the 3 - 9 keV profile. The pulse profile around the cyclotron line at 43 keV (38 - 48 keV) is not different from those at lower energies (18 - 28 keV and 28 - 38 keV), which is unlike some other pulsars that show abrupt changes in the shapes of the pulse profiles near the cyclotron line energy. For example, pulse profiles of XTE J1946+274 (Gorban et al. 2021) and 4U 1901+03 (Beri et al. 2021) show an evolution from a double-peaked to a single-peaked structure around the cyclotron line energy. Pulsations can be detected in all the energy bands as can be seen in panels (1) - (6).

3.2 Broadband Spectral Analysis

Since this particular observation has Ghost Rays contaminating the source region, as identified before, we performed the spectral analysis

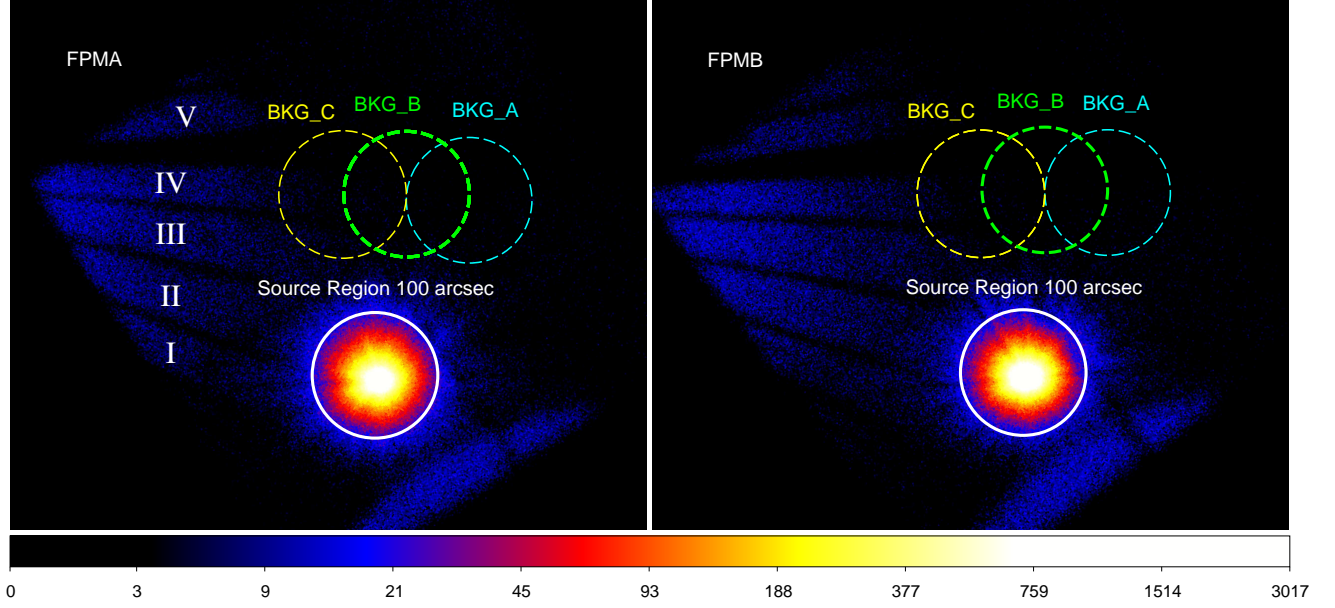


Figure 2. Image of the source gathered with FPMA (left) and FPMB (right), scaled logarithmically, are shown along with the source extraction region (white) and three different choices of background regions BKG_A (blue), BKG_B (green) and BKG_C (yellow) each of 100 arcsec radius. The five streaks seen in both FPMA and FPMB have been named using Roman Numerals.

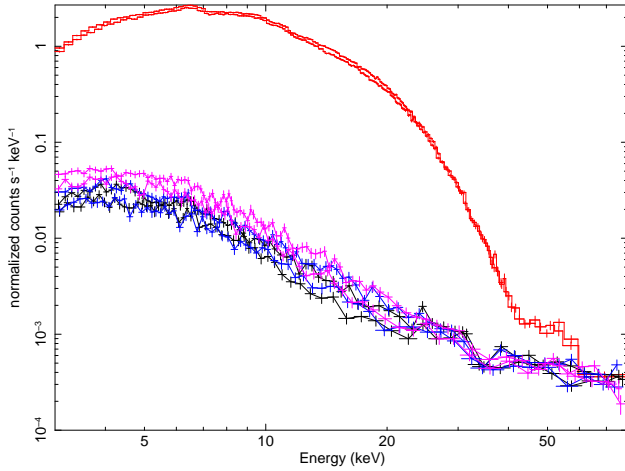


Figure 3. The **red** curves represent spectrum of the white **source** region of both FPMA and FPMB without the subtraction of the background. Similarly, the **Black**, **Blue** and **Magenta** curves represent the spectra from the regions **BKG_A**, **BKG_B** and **BKG_C** respectively (see Fig 2)

for all three choices of background regions (BKG_A, BKG_B and BKG_C). The results are not significantly affected by the choice of background as can be seen in Table. 1.

The spectrum of GRO J1750-27 resembles what is typically seen of accreting X-ray pulsars, i.e., a power-law modified by an exponential cutoff at higher energies. In order to model the continuum, we used the model, described in *XSPEC* as, $\text{const} \times \text{tbabs} \times (\text{powerlaw} * \text{highpec})$ where the *highpec* model is an exponential cut-

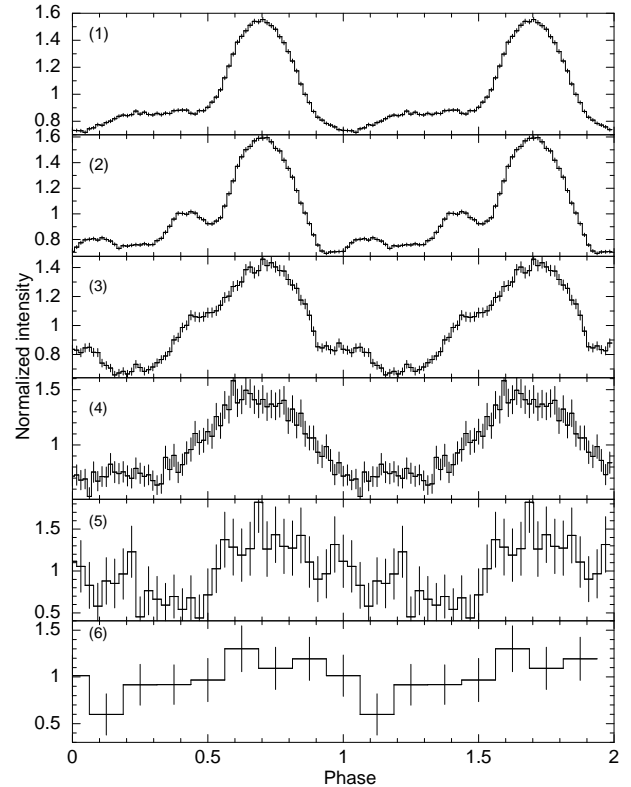


Figure 4. Energy resolved pulse profiles. The six panels represent the pulse profiles in the respective energy ranges: (1) 3 - 9 keV, (2) 9 - 18 keV, (3) 18 - 28 keV, (4) 28 - 38 keV, (5) 38 - 48 keV, (6) 48 - 65 keV

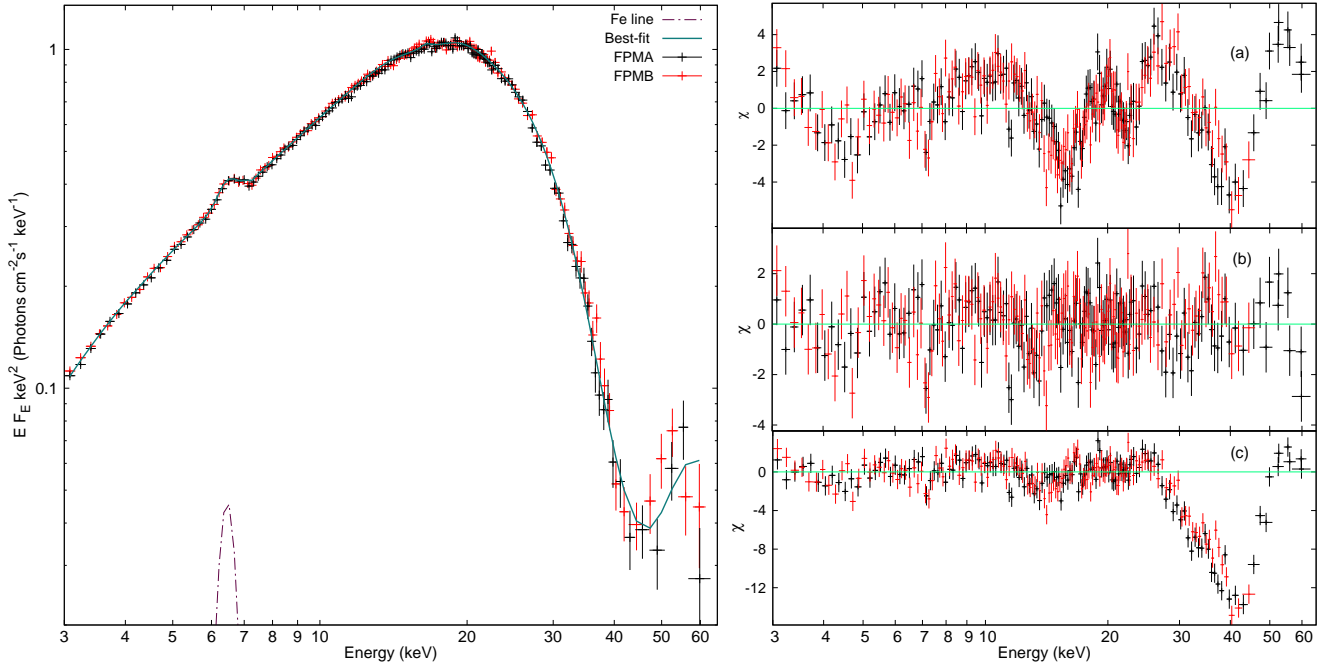


Figure 5. The unfolded spectrum with the best-fit of HighEC model is shown on the left panel. The right panel shows the residues. Panel (a) represents the residues when the continuum is fit without a "43 keV gabs" up to 65 keV. (b) is the best fit including a gabs at 43 keV and (c) is a result of fitting the continuum up to only 30 keV, but the extended range is shown. The red and black points correspond to data from FPMA and FPMB, respectively.

Table 1. Best-fitting Phase-averaged Spectral Parameters. Errors are reported at 90 % confidence.

Background	BKG_A	BKG_B	BKG_C
CB	1.012±0.003	1.013±0.003	1.013±0.003
N_H [$\times 10^{22} \text{cm}^{-2}$]	2.44 ± 0.18	2.49 ± 0.18	2.56 $^{+0.18}_{-0.18}$
Γ	0.782±0.012	0.784±0.012	0.780±0.012
Γ_{norm} [$\times 10^{-2}$]*	3.88 ± 0.11	3.90 ± 0.11	3.86 ± 0.11
E_{cut} (keV)	16.45 $^{+0.2}_{-0.22}$	16.5 $^{+0.19}_{-0.2}$	16.43 $^{+0.21}_{-0.25}$
E_{fold} kT (keV)	10.29 $^{+0.87}_{-0.6}$	10.1 $^{+0.74}_{-0.54}$	10.27 $^{+1}_{-0.613}$
E_{Fe} (keV)	6.437 ± 0.03	6.44 ± 0.03	6.44 ± 0.03
σ_{Fe} (keV)	0.2584 $^{+0.037}_{-0.035}$	0.256 $^{+0.037}_{-0.035}$	0.254 $^{+0.037}_{-0.035}$
Norm_{Fe} [$\times 10^{-4}$] [†]	7.57 $^{+0.79}_{-0.76}$	7.52 $^{+0.79}_{-0.75}$	7.42 $^{+0.70}_{-0.75}$
E_{smooth} (keV)	16.4 (fixed)	16.5 (fixed)	16.4 (fixed)
σ_{smooth} (keV)	1.6 (fixed)	1.6 (fixed)	1.6 (fixed)
τ_{smooth}	0.118 $^{+0.012}_{-0.013}$	0.122±0.012	0.119 $^{+0.012}_{-0.014}$
E_{cyc} (keV)	43.87 $^{+0.98}_{-0.78}$	43.72 $^{+0.92}_{-0.75}$	43.69 $^{+1.05}_{-0.78}$
σ_{cyc} (keV)	8.13 $^{+0.82}_{-0.65}$	7.97 $^{+0.76}_{-0.61}$	8.05 $^{+0.9}_{-0.66}$
τ_{cyc}	1.91 $^{+0.24}_{-0.18}$	1.84 $^{+0.21}_{-0.16}$	1.87 $^{+0.27}_{-0.18}$
$\chi^2(\text{dof})$ [w/o cyc]	1286(417)	1285(417)	1273(417)
$\chi^2(\text{dof})$ [w/ cyc]	487.2(414)	500.1(414)	482.9(414)
Flux [$\times 10^{-9}$] [‡]	2.225±0.007	2.225±0.007	2.225±0.007

[†]In units of photons $\text{cm}^{-2} \text{s}^{-1}$

^{*}In units of photons $\text{keV}^{-1} \text{cm}^{-2} \text{s}^{-1}$

[‡]In units of $\text{erg cm}^{-2} \text{s}^{-1}$

off¹ and tbabs accounts for the interstellar soft X-ray absorption (Wilms et al. 2000). We obtain an $N_H \sim 2.45$. This fitting resulted in an unacceptable χ^2 of 3958 for 421 d.o.f. The presence of an Fe K_{α} line at ~ 6.4 keV can be clearly seen in the spectrum and was accounted for with a gaussian emission feature. In addition, to deal with an artificial absorption like feature around the cutoff energy ($E_{\text{cut}} \sim 16.5$ keV), we used a smoothing gaussian absorption feature (gabs) with the centroid energy tied to the cutoff and the width fixed to 1.6 keV ($\sim 0.1 E_{\text{cut}}$) following the prescription suggested by Coburn et al. (2002). The inclusion of these two features reduced the χ^2 significantly to 1285 for 417 d.o.f. The residues from this fit can be seen in panel (a) of Fig. 5. Clear residues that resemble an absorption feature around 43 keV can be seen. The inclusion of a gaussian absorption model component at this energy improved the χ^2 to 500 for 414 d.o.f. The best fit model being written as $\text{const} \times \text{tbabs} \times (\text{powerlaw} \times \text{highec} + \text{gauss}) \times \text{gabs}_{\text{smooth}} \times \text{gabs}_{\text{cyc}}$. The residues after the best-fit can be seen in panel (b) of Fig. 5 and the best-fit parameters are given in Table 1. The statistical significance as a result of this large improvement of χ^2 is quite obviously high and is indicative that a gabs at 43 keV is indeed required. We interpret this feature as a cyclotron absorption feature. This feature is prominent enough that it can also be seen in the raw spectrum in Fig. 3. This feature has a width of ~ 8 keV and a large optical depth of $\tau \sim 1.9$.

The presence of the cyclotron line should be independent of the continuum parameters. To verify this we fitted the spectrum up to 30 keV with the same continuum model excluding the cyclotron absorption feature. We then extended the same model to 65 keV and the residuals from this fit can be seen in panel (c) of Fig. 5 where the extended range has been shown. Comparing panel (c) with panel (b) which represents the best fit, it can be seen that the residues are

¹ <https://heasarc.gsfc.nasa.gov/xanadu/xspec/manual/node244.html>

identical up to 30 keV. This implies that the cyclotron line feature is indeed independent of the continuum. Also, the presence of the cyclotron line is independent of the choice of background, as can be seen in Table. 1 where the model parameter values are given for different choices of background regions. We can also see from Fig. 3 that above 20 keV, all three backgrounds are comparable and therefore do not affect the cyclotron line parameters at 43 keV.

4 DISCUSSION AND CONCLUSION

Despite having discovered hundreds of Neutron Star X-ray binaries, only ~40 or so sources have been confirmed to exhibit cyclotron lines in their spectra (Staubert et al. 2019). Given that several of these are transients, it is only when they undergo outbursts that we are able to study them. This can especially be seen in the case of GRO J1750-27, where we have, only now, discovered the presence of a cyclotron line in its hard X-ray spectrum. We must keep in mind that the cyclotron lines are indicative of the magnetic field in the region where they are formed rather than the field strength at the surface of the NS. Using the 12-B-12 rule, we estimate a magnetic field strength of $B \sim 3.7 \times 10^{12}$ G for GRO J1750-27.

Another method that was used to estimate the magnetic field strength of the Neutron Star (NS) makes use of the Accretion Torque model put forward by Ghosh & Lamb (1978). The in-falling matter which has angular momentum is expected to apply a torque onto the NS at the magnetospheric radius causing the NS to either spin up or spin down. The spin change rate depends on both the period, the mass accretion rate (Luminosity) and the magnetic field strength of the NS. Therefore, by measuring the first three quantities observationally, one can estimate a field strength for the canonical NS parameters. Using this method Lutovinov et al. (2019) estimate the field strength of GRO 1750-27 to be in the range of $3.5 - 4.5 \times 10^{12}$ G. The value that we estimate is consistent with this. However, as noted by Kabiraj & Paul (2020), the estimates of the magnetic field using both these methods are not always consistent. The likely contributions could be due to the difference between the canonical NS parameters that we choose and the actual scenario. The distance uncertainty would also contribute to the uncertainty in knowing the luminosity accurately.

In addition to these factors, the cyclotron line parameters also show correlations with the luminosity of the source, and these correlations have been explained using several theories, of which the Shock-height model is one (Becker et al. 2012). This theory suggests that the height of the cyclotron line forming region varies as a function of the luminosity, where one observes a positive correlation if the NS is in the Coulombic shock regime and a negative correlation if it's in the Radiation shock regime. Depending on how close to the surface or away the line forming region is, the measured magnetic field estimate may vary. The transition between these two regimes occurs at a certain luminosity, termed the critical luminosity, L_{crit} . Sources such as V0332+53 (Lutovinov et al. 2015) and A0535+26 (Ballhausen et al. 2017; Kong et al. 2021) have been observed over a large range of luminosities and have shown a transition from a positive to a negative correlation. Studying cyclotron line sources over large luminosity ranges help in gaining a deeper understanding of the accretion onto the NS. Sources like Her X-1 (Staubert et al. 2020) also show long term evolution of the cyclotron line, which could be indicative of the local field configuration at the poles of the NS as calculated by Mukherjee & Bhattacharya (2012).

GRO J1750-27 is a relatively poorly studied source, and we have presented the discovery of a cyclotron line in this source. We estimate

a flux of $2.2 \times 10^{-9} \text{ erg cm}^{-2} \text{ s}^{-1}$ in the 3 - 79 keV range from this *NuSTAR* observation. Lutovinov et al. (2019) estimate the distance to this source to be between 14 - 22 kpc. Assuming the distance to be ~ 18 kpc, we estimate the luminosity to be, $L_X \sim 1.7 \times 10^{37} \text{ erg s}^{-1}$. The *NuSTAR* observation was made during the rising phase of the outburst, and the source continued to brighten till it reached twice this brightness when it peaked, as can be seen in Fig. 1. A transition in the accretion regime may be determined if the source were to be observed over the course of future outbursts by *NuSTAR* and other future hard X-ray missions.

ACKNOWLEDGEMENTS

This research made use of data obtained with *NuSTAR*, a project led by Caltech, funded by NASA and managed by NASA/JPL, and it utilised the NUSTARDAS software package, jointly developed by the ASDC (Italy) and Caltech (USA).

DATA AVAILABILITY

The data used in this paper are accessible through NASA's HEASARC website.

REFERENCES

- Ballhausen R., et al., 2017, *A&A*, **608**, A105
- Becker P. A., et al., 2012, *A&A*, **544**, A123
- Beri A., Girdhar T., Iyer N. K., Maitra C., 2021, *MNRAS*, **500**, 1350
- Coburn W., Heindl W. A., Rothschild R. E., Gruber D. E., Kreykenbohm I., Wilms J., Kretschmar P., Staubert R., 2002, *ApJ*, **580**, 394
- Finger M. H., Wilson-Hodge C. A., 2014, The Astronomer's Telegram, **6839**, 1
- Ghosh P., Lamb F. K., 1978, *ApJ*, **223**, L83
- Gorban A. S., Molkov S. V., Tsygankov S. S., Lutovinov A. A., 2021, *Astronomy Letters*, **47**, 390
- Harrison F. A., et al., 2013, *The Astrophysical Journal*, **770**, 103
- Kaastra J. S., Bleeker J. A. M., 2016, *A&A*, **587**, A151
- Kabiraj S., Paul B., 2020, *MNRAS*, **497**, 1059
- Koh T., Chakrabarty D., Prince T. A., Vaughan B., Zhang S. N., Scott M., Finger M. H., Wilson R. B., 1995, *IAU Circ.*, **6222**, 1
- Kong L. D., et al., 2021, arXiv e-prints, p. arXiv:2108.02485
- Lutovinov A. A., Tsygankov S. S., Suleimanov V. F., Mushtukov A. A., Doroshenko V., Nagirner D. I., Poutanen J., 2015, *MNRAS*, **448**, 2175
- Lutovinov A. A., Tsygankov S. S., Karasev D. I., Molkov S. V., Doroshenko V., 2019, *MNRAS*, **485**, 770
- Madsen K. K., Christensen F. E., Craig W. W., Forster K. W., Grefenstette B. W., Harrison F. A., Miyasaka H., Rana V., 2017, *Journal of Astronomical Telescopes, Instruments, and Systems*, **3**, 044003
- Malacaria C., Jenke P., Wilson-Hodge C., 2021, The Astronomer's Telegram, **14930**, 1
- Mukherjee D., Bhattacharya D., 2012, *MNRAS*, **420**, 720
- Reig P., 2011, *Ap&SS*, **332**, 1
- Rouco Escorial A., Wijnands R., Ootes L. S., Degenaar N., Snelders M., Kaper L., Cackett E. M., Homan J., 2019, *A&A*, **630**, A105
- Scott D. M., Finger M. H., Wilson R. B., Koh D. T., Prince T. A., Vaughan B. A., Chakrabarty D., 1997, *ApJ*, **488**, 831
- Shaw S. E., Hill A. B., Kuulkers E., Brandt S., Chenevez J., Kretschmar P., 2009, *MNRAS*, **393**, 419
- Staubert R., et al., 2019, *A&A*, **622**, A61
- Staubert R., et al., 2020, *A&A*, **642**, A196
- Wilms J., Allen A., McCray R., 2000, *ApJ*, **542**, 914

This paper has been typeset from a \TeX/L\AA\TeX file prepared by the author.